Flows with fractional quantum circulation in Bose-Einstein condensates induced by nontopological phase defects

Toshiaki Kanai,[1] Wei Guo,[2,3,*] and Makoto Tsubota[1,4]

[1]*Department of Physics, Osaka City University, 3-3-138 Sugimoto, Sumiyoshi-Ku, Osaka 558-8585, Japan*
[2]*National High Magnetic Field Laboratory, 1800 East Paul Dirac Drive, Tallahassee, Florida 32310, USA*
[3]*Mechanical Engineering Department, Florida State University, Tallahassee, Florida 32310, USA*
[4]*OCU Advanced Research Institute for Natural Science and Technology (OCARINA), Osaka City University, 3-3-138 Sugimoto, Sumiyoshi-Ku, Osaka 558-8585, Japan*

(Received 15 August 2017; published 16 January 2018)

It is a common view that rotational motion in a superfluid can exist only in the presence of topological defects, i.e., quantized vortices. However, in our numerical studies on the merging of two concentric Bose-Einstein condensates with axial symmetry in two-dimensional space, we observe the emergence of a spiral dark soliton when one condensate has a nonzero initial angular momentum. This spiral dark soliton enables the transfer of angular momentum between the condensates and allows the merged condensate to rotate even in the absence of quantized vortices. Our examination of the flow field around the soliton strikingly reveals that its sharp endpoint can induce flow like a vortex point but with a fraction of a quantized circulation. This interesting nontopological "phase defect" may generate broad interest since rotational motion is essential in many quantum transport processes.

DOI: 10.1103/PhysRevA.97.013612

I. INTRODUCTION

The hydrodynamics of quantum fluids such as atomic Bose-Einstein condensates (BECs) and superfluid helium are strongly affected by quantum effects [1–3]. For instance, it is well known that in a simply connected quantum fluid, rotational motion can arise only through the formation of topological defects in the form of quantized vortices, each of which carries a circulation of $\kappa = h/m$, where h is Planck's constant and m is the mass of the particles that form the condensate. In BECs, quantized vortices have been nucleated by a variety of innovative methods, such as direct phase imprint [4,5], rotation of the condensate traps [6–9], stirring the BECs with laser beams [10] or moving optical obstacles [11,12], decay of dark solitons [13,14], and merging isolated condensates [15]. The last method is particularly interesting since it provides a means to test the celebrated Kibble-Zurek mechanism [16,17]. This mechanism explains that the formation of vortices following a rapid second-order phase transition is due to the merging of isolated superfluid domains with random relative phases [18,19]. In addition, understanding the processes involved in the merging of isolated condensates is important for matter wave interferometry research [20–23].

So far, many studies on condensate merging have focused on condensates with uniform initial phases. However, the situation is less clear when some condensates contain vortices and carry angular momentum before merging occurs. Many interesting questions arise. For instance, how is the angular momentum transferred from a rotating condensate to an initially static condensate? Is this transfer accompanied by the transfer of vortices? Can vortices emerge at the interface between two condensates, as they can in classical shear flows? These questions have motivated us to study the intriguing merging process of a simple condensate configuration: a disk condensate with a concentric ring condensate in two-dimensional (2D) space, with one of them undergoing rotation induced by a single vortex point at the center. We shall report in this paper the observation of a spiral dark soliton during the merging, which enables angular momentum transfer and rotation in the condensates even in the absence of quantized vortices. The soliton geometry leads to a sharp endpoint of the soliton stripe. More strikingly, an examination of the velocity field around the spiral soliton reveals that its sharp endpoint can induce rotational motion in the condensate just like a vortex point but with *a fraction of a quantized circulation*. This induced flow is the essential underlying mechanism for the observed angular momentum transfer. We shall also discuss how this mechanism may play a role in 3D condensates.

II. NUMERICAL MODEL

The merging process of 2D BECs at zero temperature can be accurately described by the nonlinear 2D Gross-Pitaevskii equation (GPE) [24]:

$$i\hbar\frac{\partial\psi}{\partial t} = \left[-\frac{\hbar^2}{2m}\nabla^2 + V(\mathbf{r},t) + g|\psi|^2\right]\psi, \qquad (1)$$

where ψ is the condensate wave function, V is the external potential, and g is the coupling constant that measures the strength of the interatomic interactions. This GPE can be reduced to a dimensionless form by rescaling the parameters as $r = \xi\tilde{r}$, $t = (\hbar/ng)\tilde{t}$, and $\psi = (\sqrt{N}/\xi)\tilde{\psi}$, where $\xi = \hbar/\sqrt{2mng}$ is the healing length, $N = \int dS|\psi|^2$ is the total number of particles, and $n = N/S$ is the particle number density averaged over the

*wguo@magnet.fsu.edu

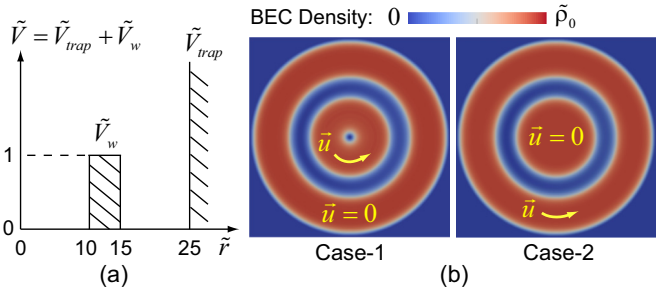

FIG. 1. (a) Schematic of the potential $\tilde{V}(\tilde{\mathbf{r}},\tilde{t})$ used in the GPE simulation. (b) The initial configurations of the Bose-Einstein condensates.

system area S:

$$i\frac{\partial\tilde{\psi}}{\partial\tilde{t}} = [-\tilde{\nabla}^2 + \tilde{V}(\tilde{\mathbf{r}},\tilde{t}) + \tilde{g}|\tilde{\psi}|^2]\tilde{\psi}. \quad (2)$$

In this dimensionless GPE, the coupling constant $\tilde{g} = N/(n\xi^2)$ equals to the dimensionless system area S/ξ^2 (i.e., about 2×10^3), and the potential $\tilde{V} = V/ng$ measures the ratio of the external potential V to the interatomic interaction strength (ng). In our simulation, we set $\tilde{V} = \tilde{V}_{\rm trap} + \tilde{V}_w$, where $\tilde{V}_{\rm trap}$ represents the cylindrical hard-wall box potential of the trap and $\tilde{V}_w$ denotes the potential barrier that separates the disk and the ring condensates as shown in Fig. 1(a). The condensates are confined by $\tilde{V}_{\rm trap}$ to have an outer radius of 25ξ. This condensate size is within the range of typical condensate sizes in real experiments (i.e., about 10ξ–$10^2\xi$ [12,15,25,26]). The value of $\tilde{V}_w$ depends on the atomic species, number density, and the frequency and power flux of the laser beams for trapping or separating the condensates, which is typically in the range of $1-10^2$ [12,15,25–28]. Here we present our simulation results with $\tilde{V}_w = 1$. We have checked that further increasing $\tilde{V}_w$ does not alter the essential physics.

Two specific initial configurations of the condensates are considered in our numerical study. In case 1, the inner disk condensate contains a single vortex point at its center while the outer ring condensate is static. In case 2, the outer ring condensate carries a supercurrent with one quantum of circulation κ while the inner disk condensate is static. By evolving Eq. (2) in imaginary time [29], the steady initial condensate profiles are achieved and are shown in Fig. 1(b). At time $\tilde{t} = 0$, we then suddenly remove the energy barrier $\tilde{V}_w$ and let the two condensates merge. These condensate configurations are different from those used in some early BEC interference experiments [9,30] but they can still be easily realized. For instance, Corman *et al.* [26] and Eckel *et al.* [31] have utilized the interference patterns of a ring condensate and a disk condensate during free expansion to study the Kibble-Zurek mechanism and superfluid weak links. Their setup can be easily adapted to examine the results of our simulation.

III. SIMULATION RESULTS

We carried out our simulation in a region $\tilde{\mathbf{r}} \in [-25,25] \times [-25,25]$ with a mesh grid of 500×500 nodes to ensure spatial convergence. The time step δ_t is chosen to be 1.0×10^{-4}. The evolution of the condensate wave function during merging is

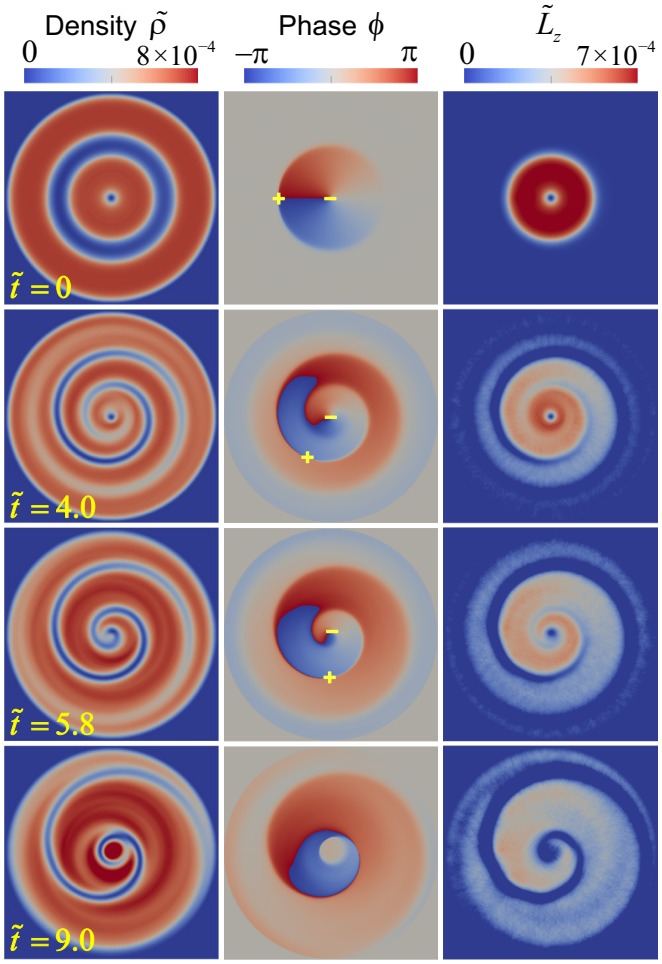

FIG. 2. Case 1 representative snapshots showing the time evolution of the BEC density, phase, and angular momentum density $\tilde{L}_z$. The "+" and "−" signs indicate the locations of the positive and negative vortex points.

obtained by numerically integrating Eq. (2) using an alternating direction implicit method [32]. Representative snapshots of the dynamical evolution of the dimensionless condensate density $\tilde{\rho} = |\tilde{\psi}|^2$ and phase ϕ, following the removal of the potential barrier $\tilde{V}_w$, are shown for case 1 in Fig. 2 and for case 2 in Fig. 3. In both cases, we observe the emergence of a spiral stripe with depleted condensate density and with an abrupt phase step $\triangle\phi$ across the stripe boundary. This stripe is indeed a dark soliton, similar in nature to the ring dark solitons identified in the expansion of disk and annular condensates in two-dimensional space [33–35]. The boundary of the soliton moves at a speed that is determined by the phase step. For $\triangle\phi = \pi$, the soliton has zero velocity, zero density at its center, and has a width on the order of ξ. When $\triangle\phi$ decreases, the soliton becomes shallower and wider, and its speed increases [36]. The unique spiral shape of the dark soliton seen in our simulation is due to the relative phases between the initial disk and ring condensates. For instance, in case 1, the ring condensate has a uniform phase while the inner disk has a phase winding of 2π. There is a point across which the relative phase between the disk and the ring condensates changes sign. The soliton then develops two ends, with one end spiraling in and the other

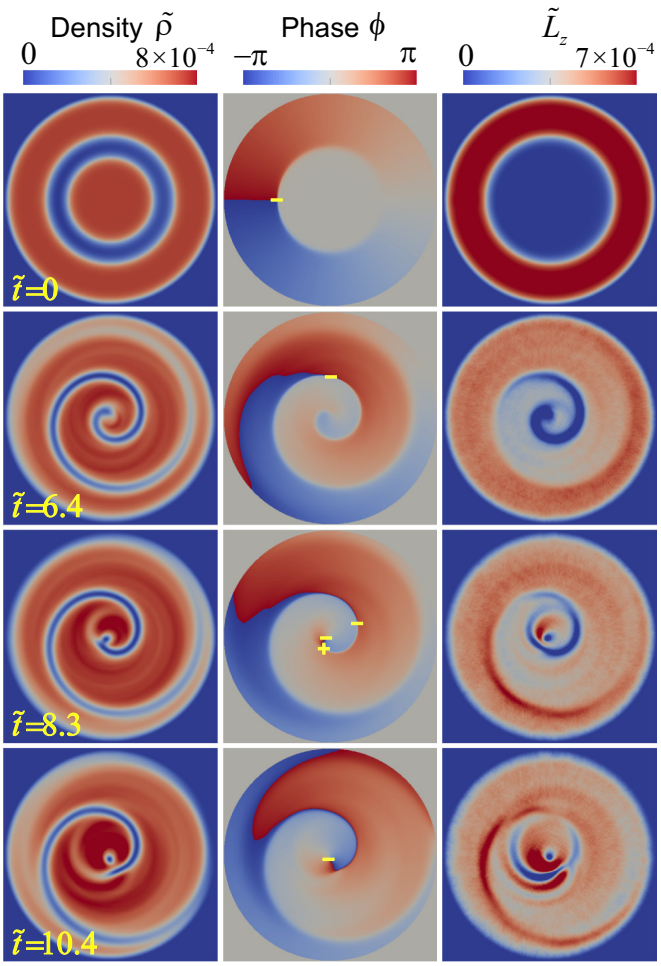

FIG. 3. Case 2 representative snapshots showing the time evolution of the BEC density, phase, and angular momentum density $\tilde{L}_z$. The "+" and "−" signs indicate the locations of the positive and negative vortex points.

extending out. The different chirality of the spiral solitons in cases 1 and 2 indeed reflects the different relative phase winding between the two condensates.

Interesting interactions between the spiral dark soliton and quantized vortex points are also observed. We first note that besides the physical vortices, the terminal point of the phase branch-cut line is deemed as a phase vortex in GPE simulation that does not induce rotational flow, but has a phase winding of 2π around it. In both cases, the dark soliton stripe quickly develops a sharp inner end that spirals toward the center of the condensate. In case 1, at about $\tilde{t} = 5.8$, the negative vortex point initially located at the center merges into the dark soliton. Subsequently, this vortex point moves along the soliton stripe and annihilates with the positive phase vortex, rendering the condensate completely vortex free, as depicted in Fig. 2 at $\tilde{t} = 9.0$. In case 2, as the sharp inner end spirals in, the local curvature radius of the soliton stripe becomes comparable to ξ. Snake instability then occurs [37–39] and a pair of positive and negative vortex points are nucleated at $\tilde{t} = 7.2$. The negative vortex point peels off from the soliton while the positive one sits inside the stripe (see Fig. 3 at $\tilde{t} = 8.3$). This positive vortex point then moves along the soliton stripe and annihilates with the phase

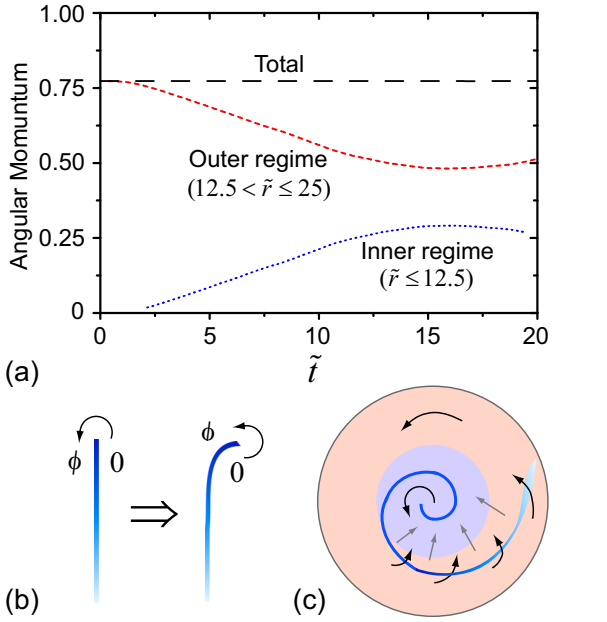

FIG. 4. (a) The time evolution of the integrated angular momentum for case 2. (b) Schematic diagrams showing how the sharp endpoint of a dark soliton stripe can induce rotational motion in a condensate and how such motion bends the soliton stripe. (c) Schematics illustrating the mass and angular momentum transfer in case 2.

vortex, leaving the condensate with one single negative vortex point at the center. In long time evolution, the solitons in both cases eventually decay into vortices via snake instability [40].

We have also studied the time evolution of the dimensionless angular momentum density $\tilde{L}_z$, defined as

$$\tilde{L}_z = \frac{\xi^2}{\hbar N}(\psi^* \hat{L}_z \psi) = \frac{1}{i}\tilde{\psi}^* \left(\tilde{x}\frac{\partial}{\partial \tilde{y}} - \tilde{y}\frac{\partial}{\partial \tilde{x}} \right) \tilde{\psi}. \qquad (3)$$

As shown in Figs. 2 and 3, the angular momentum initially is confined to the rotating condensate. During the merging, the angular momentum spreads to the initially static condensate region along the spiral channel formed by the soliton stripe. The time evolution of the integrated dimensionless angular momentum, for case 2 as an example, is shown in Fig. 4(a). We see clearly that the angular momentum is transferred from the outer ring region ($12.5 < \tilde{r} \leqslant 25$) to the inner disk region ($\tilde{r} \leqslant 12.5$) while the total angular momentum is conserved. One may think that this transfer occurs naturally as the condensate flows from the rotating region through the spiral channel to the initially static region. However, this is not true. In case 2, the flow in the initially rotating condensate is counterclockwise, so it cannot enter the outward spiral channel formed by the soliton. The situation is similar for case 1. Therefore, the rotation in the initially static condensate must be induced by a different mechanism that is effective even without vortices.

IV. DISCUSSIONS

Observing the abrupt phase step $\triangle\phi$ across the dark soliton boundary, we realize that for a soliton stripe with a sharp endpoint, there must also be a phase winding of $\triangle\phi$ around this endpoint, as illustrated in Fig. 4(b). Such a phase winding

actually leads to a rotational motion in the condensate, making the sharp endpoint effectively a "vortex point" that carries a fraction of a quantized circulation given by $(\frac{\triangle\phi}{2\pi})\kappa$. Note that mathematically the circulation (i.e., integral of the velocity around the endpoint) is still zero due to the opposite phase velocity inside the soliton density-depleted region. When the soliton is nearly black (i.e., $\triangle\phi \to \pi$), mass flow through the soliton boundary is prohibited. In this case, the flow induced by the sharp endpoint transports condensate mass from one side of the soliton stripe to the other side, which leads to spontaneous curving of the sharp end of the soliton stripe. Now the mechanism for the observed angular momentum transfer can be identified. Let us again consider case 2. As shown in Fig. 4(c), the inner sharp end of the spiral soliton moves toward the center and induces a counterclockwise flow in the inner region, allowing the inner condensate to rotate. This induced flow carries the condensate mass from the inner region to the outer region, guided by the spiral channel. Meanwhile, this outward flow leads to a phase increment along the soliton boundary, which consequently causes a phase gradient along the radial direction that drives an inward mass flow (see the phase plot at $\tilde{t} = 6.4$ in Fig. 3). In the shallow tail part of the soliton stripe, the condensate density in the soliton is not depleted and mass flow from the outer region through the soliton boundary toward the inner region becomes significant. As a consequence, a mass circulation between the inner and the outer regions is formed in the condensate, which effectively mixes the condensate and transports angular momentum between these two regions.

To support our model, we have examined quantitatively the flow field around the spiral dark soliton. Let us take the snapshot in case 2 at $\tilde{t} = 6.4$ as an example, since in this case the flow induced by the sharp inner endpoint of the soliton is not affected by any nearby physical vortices and there is a clear phase winding around the endpoint. To focus on the rotational motion, we introduce a vortex charge parameter Z, defined as $Z = \frac{m}{\hbar}|\mathbf{r} \times \mathbf{v}(\mathbf{r})| = \frac{m}{\hbar} r v_\theta$, where v_θ is the velocity along the azimuthal angle direction. For a flow field induced by a vortex point at the origin, Z is constant everywhere and equals the winding number of the vortex. We have calculated the Z values in the condensate along the solid lines as shown in Fig. 5. The error bars represent the variations of Z along these solid lines. The small variation of Z suggests that v_θ scales as $1/r$ along these lines. We see that near the sharp inner endpoint, the Z values are about 0.4, which indeed matches well with the measured phase step across the soliton boundary near the endpoint (i.e., $\triangle\phi \simeq 0.8\pi$). The flow induced by the endpoint in this region is protected. This is because the soliton has fairly depleted density close to the inner endpoint, and consequently mass flow from the outer region is strongly prohibited. In areas where there are appreciable mass flows across the soliton boundary from the outer region, Z starts to increase and approaches one, a value that is expected for the flow in the initial outer ring condensate.

We have also studied the merging of the two condensates with various other initial conditions. For instance, when the outer ring condensate initially carries a supercurrent with a winding number greater than one, multiple spiral solitons are created, and the number of solitons matches the winding number. For the case that there is no rotation in the two condensates, ring-shaped solitons, instead of spiral solitons, are observed.

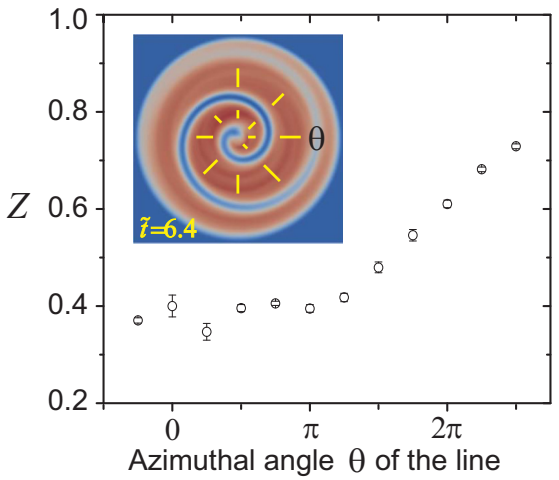

FIG. 5. Variation of the calculated vortex charge number Z in the condensate along the solid yellow lines that are shown in the inset.

In three-dimensional (3D) condensates, similar flows around soliton edges should also exist. For instance, a disk-shaped soliton with a sharp edge should have a phase winding around its edge that induces flows in the condensate, which is effectively like a vortex ring but with a fractional quantum circulation that matches the phase step across the soliton disk. Shomroni *et al.* have reported the creation of disk dark solitons in 3D cigar-shaped condensates [41]. However, in those experiments the soliton edge is on the BEC surface, which renders no visible rotational motion in the condensate. Nevertheless, in our recent study on the merging of a 3D rotating cylindrical condensate with a static cylindrical condensate, a helical soliton sheet is observed whose sharp leading edge is seen to induce flows like a vortex line, which confirms that the mechanism we identified in 2D condensates also exists in 3D systems. More details of this study will be reported in a later publication.

V. SUMMARY

In summary, our study has revealed that sharp end points or edges of dark solitons in BECs are nontopological phase defects that can induce rotational motion in the condensates like vortices. The flows induced by these nontopological defects carry a fraction of a quantized circulation that matches the phase step across the soliton boundary. This mechanism is critical in transferring angular momentum and condensate mass in the merging of rotating condensates. It may also play important roles in other quantum transport processes and in quantum turbulence [42] where rotational motion is essential.

ACKNOWLEDGMENTS

W.G. acknowledges the support from the National Science Foundation under Grant No. DMR-1507386. W.G. is also thankful for the support from the Japan Society for the Promotion of Science (JSPS) through the Invitational Fellowship Program (No. S17018) and to Osaka City University for hosting his visit. M.T. would like to acknowledge the support by JSPS KAKENHI under Grants No. JP17K05548 and No. JP16H00807.

[1] A. Fetter and A. Svidzinsky, J. Phys.: Condens. Matter **13**, R135 (2001).

[2] R. J. Donnelly, *Quantized Vortices in Helium II* (Cambridge University Press, Cambridge, UK, 1991).

[3] M. Tsubota, M. Kobayashi, and H. Takeuchi, Phys. Rep. **522**, 191 (2013).

[4] M. R. Matthews, B. P. Anderson, P. C. Haljan, D. S. Hall, C. E. Wieman, and E. A. Cornell, Phys. Rev. Lett. **83**, 2498 (1999).

[5] A. E. Leanhardt, A. Görlitz, A. P. Chikkatur, D. Kielpinski, Y. Shin, D. E. Pritchard, and W. Ketterle, Phys. Rev. Lett. **89**, 190403 (2002).

[6] E. Hodby, G. Hechenblaikner, S. A. Hopkins, O. M. Maragò, and C. J. Foot, Phys. Rev. Lett. **88**, 010405 (2001).

[7] J. R. Abo-Shaeer, C. Raman, J. M. Vogels, and W. Ketterle, Science **292**, 476 (2001).

[8] P. C. Haljan, I. Coddington, P. Engels, and E. A. Cornell, Phys. Rev. Lett. **87**, 210403 (2001).

[9] S. Inouye, S. Gupta, T. Rosenband, A. P. Chikkatur, A. Görlitz, T. L. Gustavson, A. E. Leanhardt, D. E. Pritchard, and W. Ketterle, Phys. Rev. Lett. **87**, 080402 (2001).

[10] K. W. Madison, F. Chevy, W. Wohlleben, and J. Dalibard, Phys. Rev. Lett. **84**, 806 (2000).

[11] K. Sasaki, N. Suzuki, and H. Saito, Phys. Rev. Lett. **104**, 150404 (2010).

[12] W. J. Kwon, J. H. Kim, S. W. Seo, and Y. Shin, Phys. Rev. Lett. **117**, 245301 (2016).

[13] Z. Dutton, M. Budde, C. Slowe, and L. V. Hau, Science **293**, 663 (2001).

[14] B. P. Anderson, P. C. Haljan, C. A. Regal, D. L. Feder, L. A. Collins, C. W. Clark, and E. A. Cornell, Phys. Rev. Lett. **86**, 2926 (2001).

[15] D. R. Scherer, C. N. Weiler, T. W. Neely, and B. P. Anderson, Phys. Rev. Lett. **98**, 110402 (2007).

[16] C. N. Weiler, T. W. Neely, D. R. Scherer, A. S. Bradley, M. J. Davis, and B. P. Anderson, Nature (London) **455**, 948 (2008).

[17] R. Carretero-González, B. P. Anderson, P. G. Kevrekidis, D. J. Frantzeskakis, and C. N. Weiler, Phys. Rev. A **77**, 033625 (2008).

[18] W. H. Zurek, Phys. Rep. **276**, 177 (1996).

[19] T. W. B. Kibble, Phys. Today **60**, 47 (2007).

[20] Y. Shin, M. Saba, T. A. Pasquini, W. Ketterle, D. E. Pritchard, and A. E. Leanhardt, Phys. Rev. Lett. **92**, 050405 (2004).

[21] Z. Hadzibabic, S. Stock, B. Battelier, V. Bretin, and J. Dalibard, Phys. Rev. Lett. **93**, 180403 (2004).

[22] T. Yang, B. Xiong, and K. A. Benedict, Phys. Rev. A **87**, 023603 (2013).

[23] B. Xiong, T. Yang, and K. A. Benedict, Phys. Rev. A **88**, 043602 (2013).

[24] L. P. Pitaevskii and S. Stringari, *Bose-Einstein Condensation* (Oxford University Press, Oxford, UK, 2003).

[25] F. Jendrzejewski, S. Eckel, N. Murray, C. Lanier, M. Edwards, C. J. Lobb, and G. K. Campbell, Phys. Rev. Lett. **113**, 045305 (2014).

[26] L. Corman, L. Chomaz, T. Bienaimé, R. Desbuquois, C. Weitenberg, S. Nascimbène, J. Dalibard, and J. Beugnon, Phys. Rev. Lett. **113**, 135302 (2014).

[27] T. C. Killian, D. G. Fried, L. Willmann, D. Landhuis, S. C. Moss, T. J. Greytak, and D. Kleppner, Phys. Rev. Lett. **81**, 3807 (1998).

[28] A. L. Gaunt, T. F. Schmidutz, I. Gotlibovych, R. P. Smith, and Z. Hadzibabic, Phys. Rev. Lett. **110**, 200406 (2013).

[29] M. L. Chiofalo, S. Succi, and M. P. Tosi, Phys. Rev. E **62**, 7438 (2000).

[30] Y. Shin, C. Sanner, G.-B. Jo, T. A. Pasquini, M. Saba, W. Ketterle, D. E. Pritchard, M. Vengalattore, and M. Prentiss, Phys. Rev. A **72**, 021604 (2005).

[31] S. Eckel, F. Jendrzejewski, A. Kumar, C. J. Lobb, and G. K. Campbell, Phys. Rev. X **4**, 031052 (2014).

[32] W. H. Press, B. P. Flannery, S. A. Teukolsky, and W. T. Vetterling, *Numerical Recipes in C: The Art of Scientific Computing* (Cambridge University Press, Cambridge, UK, 1992).

[33] S. J. Yang, Q. S. Wu, S. N. Zhang, S. Feng, W. Guo, Y. C. Wen, and Y. Yu, Phys. Rev. A **76**, 063606 (2007).

[34] S. J. Yang, Q. S. Wu, S. Feng, Y. C. Wen, and Y. Yu, Phys. Rev. A **77**, 035602 (2008).

[35] L. A. Toikka, O. Kärki, and K.-A. Suominen, J. Phys. B **47**, 021002 (2014).

[36] A. D. Jackson, G. M. Kavoulakis, and C. J. Pethick, Phys. Rev. A **58**, 2417 (1998).

[37] A. V. Mamaev, M. Saffman, and A. A. Zozulya, Phys. Rev. Lett. **76**, 2262 (1996).

[38] G. Theocharis, D. J. Frantzeskakis, P. G. Kevrekidis, B. A. Malomed, and Y. S. Kivshar, Phys. Rev. Lett. **90**, 120403 (2003).

[39] M. Ma, R. Carretero-González, P. G. Kevrekidis, D. J. Frantzeskakis, and B. A. Malomed, Phys. Rev. A **82**, 023621 (2010).

[40] See Supplemental Material at http://link.aps.org/supplemental/10.1103/PhysRevA.97.013612 for movies that show the time evolution of the condensate density and phase for the two initial configurations described in the text.

[41] I. Shomroni, E. Lahoud, S. Levy, and J. Steinhauer, Nat. Phys. **5**, 193 (2009).

[42] W. F. Vinen and J. J. Niemela, J. Low Temp. Phys. **128**, 167 (2002).